

Study of Neutron Stars as sources of continuous gravitational waves

M. Sc. Project (PHYAP650RP) Report

Submitted to

**Department of Physics,
Savitribai Phule Pune University, Pune**

For the partial fulfilment of the degree of Master of Science (M.Sc.)

In

PHYSICS

By

PUJA MANDAL

Under the supervision of

Debarati Chatterjee

Associate Professor,IUCAA.

May 2025

CERTIFICATE

PHY-C475 / PHY 650RP

*This is to certify that the project report entitled “**Study of Neutron Stars as sources of continuous gravitational waves**” is completed by **Puja Mandal** (Seat No 23024011) for the partial fulfilment of the requirement of the degree of Master of Science in Physics of Savitribai Phule Pune University, Pune. This work is original and not submitted before for any other degree at this or any other University.*

Place: IUCAA, Pune, India

Date:

Name of Guide: Debarati Chatterjee

Signature of Guide: 

Project Guide/Internal guide,
Department of Physics,
Savitribai Phule Pune University, Pune, 411007.

Head

*Department of Physics
Savitribai Phule Pune University,
Pune, 411007*

DECLARATION

PHY-C475 / PHY 650RP

I hereby declare that the project work entitled "**Study of Neutron Stars as sources of continuous gravitational waves**" submitted for the partial fulfilment of the degree of Master of Science in Department of Physics, Savitribai Phule Pune University, Pune; is carried out by me and has not been previously formed on the basis for the award of any degree or diploma or another similar title of this or any other University.

Place: IUCAA, Pune, India

Date: 20/05/2025

Name of the student : Puja Mandal
Signature:

Seat No. 23024011

Study of Neutron Stars as sources of Continuous Gravitational Waves

Puja Mandal

May 20, 2025

Abstract

Rapidly spinning neutron stars (NS) with non-axisymmetric deformations can be sources of continuous gravitational waves (GW). However such signals are much weaker than those compared to compact binary merger events, and have not yet been observed with the existing gravitational wave detectors. In this project, we explore the mechanism of emission of continuous GW,

1 Introduction

1.1 Background

Neutron stars are extraordinary astronomical objects formed as the remnants of massive stars after they undergo a supernova explosion. These compact stars are characterized by their extremely high densities, often exceeding that of atomic nuclei, and possess some of the strongest gravitational and magnetic fields in the universe. Neutron stars typically have a radius of about 10-12 km and a mass ranging from 1.1 to about 2.3 times the mass of the Sun. The internal structure of neutron stars is determined by the equation of state (EOS), which describes the relationship between pressure, density, and energy in such extreme conditions. However, the exact EOS for dense nuclear matter remains an area of active research due to uncertainties in understanding the behavior of matter at ultra-high densities. Observations of neutron star properties, such as mass, radius, and rotational frequencies, help constrain these theoretical models. For example, recent measurements of gravitational waves from binary neutron star mergers have provided new insights into their structural characteristics and physical properties, including potential phase transitions from hadronic to quark matter within their cores [1, 2].

The neutron star appears at the end phase of the evolution of massive stars ($M > 8M_{\odot}$). At this stage, most of these stars have grown an iron core that cannot be supported by hydrostatic pressure and it leads to a collapse of the star. In most of the cases it produces supernovae (SN), releasing gravitational energy of about 10^{53} ergs and leading to the complete destruction of the progenitor star. SN leaves behind compact remnants such as neutron stars and black holes. During the supernova, the core of the star collapses under gravity, compressing protons and electrons into neutrons. This collapse stops when the core reaches neutron degeneracy pressure, a quantum pressure that halts further collapse and stabilizes the core as a neutron star. A star with an initial mass between approximately $8M_{\odot} - 25M_{\odot}$ is likely to form a neutron star after going supernova. Stars with initial masses above approximately $20M_{\odot} - 25M_{\odot}$ are more likely to leave behind black holes. However, the precise mass limit is not fully determined, as it depends on factors like metallicity, rotation, and mass loss through stellar winds.

Compact stars such as neutron stars are unique laboratories that allow us to probe the building blocks of matter and their interactions at regimes complementary to terrestrial laboratories. These exceptionally complex astrophysical sources have already led to various breakthrough discoveries in nuclear and subnuclear physics. The most recent one being the detection of gravitational wave detection from merging of two neutron stars in 2017 (GW170817) . These observations commenced the multi messenger astronomy with simultaneous detection of gravitational waves and their electromagnetic counterparts (in X-rays, Gamma-rays, radio waves etc) from the same event. The detection of emission

from the binary neutron star merger has led to fundamental discoveries due to the fact that it is the possible site of nucleosynthesis of new radioactive elements and the production of new states of matter [3].

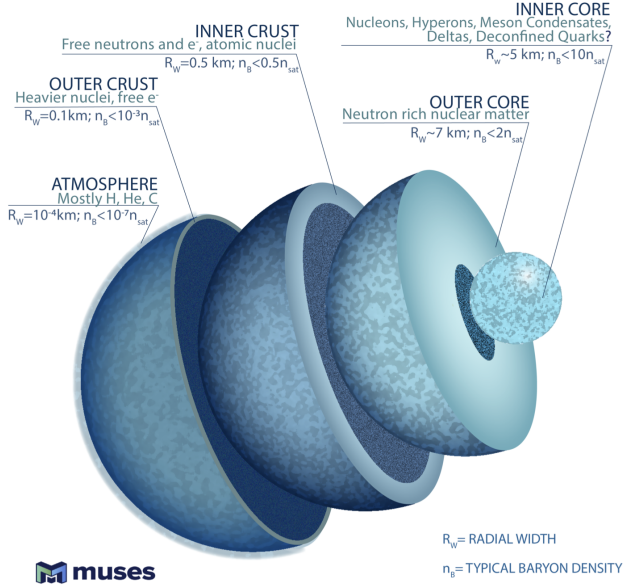


Figure 1: Internal structure of a neutron star [4].

1.2 Neutron star structure

The density and pressure increase with increasing depth in an NS. The dense, liquid core lies beneath the solid crust, which is covered by a thin envelope and a very thin atmosphere. The core constitutes the largest part of the neutron star, approximately 99% of the total mass, and may be subdivided into an outer and an inner part. The outer core occupies the density range $\rho \approx (1-2)\rho_0$. It is composed primarily of degenerate neutrons and merely a few percent of protons and electrons. Both protons and neutrons are expected to be superfluid in the outer core. In the inner core of the neutron star, the density may become as $\rho \approx (8-10)\rho_0$, depending on the model of the interior. It may become energetically favorable for more exotic particles, rather than the standard composition of p, e^-, n to appear at these high densities. Going from the centre towards the outer edge, we encounter the crust. The crust typically covers about one tenth of the neutron star radius and can be subdivided into an inner and an outer part. The outer crust extends from the bottom of the atmosphere to the neutron drip density, $\rho_{\text{drip}} \approx 4.3 \times 10^{11} \text{ g cm}^{-3}$. Matter consists of electrons and ions in the outer crust. Due to the rise in electron Fermi energy, the nuclei

suffer inverse β -decay and become more neutron-rich with increasing density. The inner crust covers the region from the neutron drip density, where neutrons start to drip out of the nuclei, to the nuclear density and is composed of electrons, free superfluid neutrons and neutron-rich nuclei. As the density increases, the nuclei grow heavier and the number of neutrons residing in the free neutron fluid (rather than in nuclei) also increases. Nuclei begin to dissolve and merge together around what is known as the crust-core interface. The envelope or ocean refers to $\approx 100m$ thick layer that lies on top of the crust and extends to a density of $\rho \approx 10^{10} \text{ g cm}^{-3}$. The envelope/ocean couples the sought-after temperature of the (isothermal) interior T_B , to the observable effective surface temperature T_{eff} , which is then further affected by the atmosphere, the next layer of the neutron star going from centre to the outer surface. The atmosphere covers the neutron star and is very thin ($\approx cm$). It is thought to be composed of pure hydrogen (H), since heavier elements should sink on very short timescales. However, for some isolated or quiescent neutron stars, observations suggest atmospheres composed of He or C [3]

The equation of state (EOS) is the relationship between pressure and density within a neutron star, dictated by the microphysics of dense matter. This relationship defines how matter responds under immense gravitational compression, determining the star's mass-radius relation and stability limits. In the dense core of neutron stars, matter may exist in exotic forms, and thus, the EOS encompasses a range of possible states from ordinary nuclear matter to potentially deconfined quark matter. The EOS is fundamental to understanding neutron star structure and is pivotal in constraining models of dense matter based on both theoretical and observational insights [5].

The composition of a neutron star profoundly impacts its equation of state (EOS), which in turn dictates the star's structural characteristics, including its mass-radius relationship and maximum mass. In the outer crust, where matter consists of nuclei embedded in a sea of electrons, the EOS is relatively soft due to weaker nuclear interactions. Moving inward, in the region of the neutron drip, some neutrons become unbound from nuclei, increasing the pressure, which slightly stiffens the EOS. In the outer core, where densities are high enough for neutrons and protons to dominate, along with electrons and potentially muons, the EOS is strongly affected by nuclear interactions among these particles, resulting in increased resistance to gravitational compression. As densities rise further in the core, the possibility of exotic matter states, such as hyperons or even de-confined quark matter, may emerge. The appearance of such particles can soften the EOS because they allow additional degrees of freedom, which reduce the pressure for a given density and, consequently, can decrease the maximum stable mass of the neutron star. Thus, the EOS is highly dependent on the composition of matter under extreme conditions, determining not only the neutron star's structure but also its stability against collapse [5].

1.3 Quantum Degeneracy Pressure and NS EOS

Cold matter is stable against collapse, because two fermions cannot be in the same quantum state. If N electrons (or N identical fermions of any kind) are in a volume V , their average momentum is as large as if each occupied a volume V/N . (In a collection of bosons in its ground state, each boson has the ground state energy for a box of volume V .) The spacing between electrons is

$$\ell = (V/N)^{1/3} = n^{-1/3},$$

where n is the particle density, $n = N/V$. An electron confined to a box of length ℓ has a minimum momentum given by the uncertainty relation,

$$p \sim \frac{\hbar}{\ell} = hn^{1/3}.$$

Ordinary gas is too hot for the minimum momentum allowed by the uncertainty relation to be important; the particles are widely separated, and their average thermal momentum $\sim \sqrt{mkT}$, is much larger than this minimum momentum. As a result, the translational kinetic energy per particle in the thermal energy $E = \frac{3}{2}kT$, and their pressure is very close to the thermal pressure of an ideal gas, $P = nkT$. In a liquid or solid, however, the pressure is provided by the resistance of electrons against being crushed to a length smaller than their ground state spacing. In the ground state, their kinetic energy is not zero; the minimum momentum given above implies a minimum kinetic energy,

$$E = \frac{p^2}{2m} = \frac{\hbar^2}{2m} n^{2/3},$$

and the corresponding minimum pressure is

$$P = n\langle p_x v_x \rangle = \frac{1}{3}n\langle pv \rangle = \frac{p^2}{3m}n \sim \frac{\hbar^2}{m} n^{5/3}. \quad (\text{XIII.1})$$

In a metal, the outer electrons are free to move, but they are still in or near the ground state, with the spacing between electrons equal to atomic spacing. For what density n is this minimum pressure comparable to the kinetic pressure $P = nkT$? The degeneracy energy must be comparable to kT :

$$E = \frac{\hbar^2}{m} n^{2/3} = kT. \quad (\text{XIII.2})$$

At room temperature, with $m = m_e$, we have

$$n^{2/3} = \frac{kTm_e}{\hbar^2} \left(\frac{1 \text{ eV}}{kT} \right) \left[1.511 \text{ MeV} / (3 \times 10^{10} \text{ cm/s})^2 \right] \quad (\text{XIII.3})$$

$$= 3 \times 10^{13} \text{ cm}^{-2} \Rightarrow \ell = n^{-1/3} = 2 \times 10^{-7} \text{ cm}. \quad (\text{XIII.4-5})$$

Degeneracy Condition at Atomic Spacing

This is well above atomic spacing, so metals are degenerate. At atomic spacing,

$$\ell = 5 \times 10^{-9} \text{ cm},$$

matter is degenerate when

$$kT < \frac{\hbar^2}{m_e} n^{2/3} = \frac{\hbar^2}{m_e \ell^2} \sim 10 \text{ eV}, \quad (\text{XIII.6})$$

$$\Rightarrow T < 10^5 \text{ K}. \quad (\text{XIII.7})$$

10 eV is the kinetic energy of electrons confined to an atomic-size volume. (It is of the order of the binding energy — e.g., 13.6 eV for hydrogen). In particular, the Sun and Jupiter have electrons at atomic spacing (each has density of about 1 g cm^{-3}) so the Sun, with average temperature far above 10^5 K , is not degenerate, while Jupiter.[6]

Equation of State for a Cold, Degenerate Fermi Gas

Assumptions

- Zero temperature ($T = 0$): All fermions occupy states up to the Fermi momentum p_F .
- Degeneracy condition: $kT \ll E_F$, where E_F is the Fermi energy.
- Charge neutrality: $n_e = n_p$ (for neutron star matter).

Number Density

For a Fermi gas with spin degeneracy $g = 2$:

$$n = \frac{g}{(2\pi\hbar)^3} \int_0^{p_F} 4\pi p^2 dp = \frac{p_F^3}{3\pi^2\hbar^3}.$$

For electrons ($m = m_e$) and nucleons ($m = m_p, m_n$):

$$n_e = \frac{p_{F,e}^3}{3\pi^2\hbar^3}, \quad n_i = \frac{p_{F,i}^3}{3\pi^2\hbar^3} \quad (i = p, n).$$

Fermi Energy

The Fermi energy for a particle of mass m :

$$E_F = \sqrt{p_F^2 c^2 + m^2 c^4}.$$

- Non-relativistic ($p_F \ll mc$): $E_F \approx \frac{p_F^2}{2m}$.
- Ultra-relativistic ($p_F \gg mc$): $E_F \approx p_F c$.

Pressure and Energy Density

Pressure P and energy density ϵ :

$$P = \frac{g}{3(2\pi\hbar)^3} \int_0^{p_F} \frac{p^2 c^2}{\sqrt{p^2 c^2 + m^2 c^4}} 4\pi p^2 dp,$$

$$\epsilon = \frac{g}{(2\pi\hbar)^3} \int_0^{p_F} \sqrt{p^2 c^2 + m^2 c^4} \cdot 4\pi p^2 dp.$$

Dimensionless form: define $x \equiv p_F/mc$ and $\lambda_c \equiv \hbar/mc$:

$$P = \frac{mc^2}{\lambda_c^3} \phi(x), \quad \epsilon = \frac{mc^2}{\lambda_c^3} \chi(x),$$

where:

$$\phi(x) = \frac{1}{3\pi^2} \int_0^x \frac{x'^4}{\sqrt{1+x'^2}} dx', \quad \chi(x) = \frac{1}{\pi^2} \int_0^x x'^2 \sqrt{1+x'^2} dx'.$$

*Limiting Cases

- Non-relativistic ($x \ll 1$):

$$\phi(x) \approx \frac{x^5}{15\pi^2}, \quad \chi(x) \approx \frac{x^3}{3\pi^2} \left(1 + \frac{3x^2}{10}\right).$$

EOS: $P \approx \frac{\hbar^2}{5m} (3\pi^2)^{2/3} n^{5/3}$.

- Ultra-relativistic ($x \gg 1$):

$$\phi(x) \approx \frac{x^4}{12\pi^2}, \quad \chi(x) \approx \frac{x^4}{4\pi^2}.$$

EOS: $P \approx \frac{\hbar c}{4} (3\pi^2)^{1/3} n^{4/3}$.

Beta-Equilibrium in Neutron Stars

For $n \leftrightarrow p + e^- + \bar{\nu}_e$ equilibrium, the chemical potentials are related as:

$$E_F^n = E_F^p + E_F^e.$$

With $n_p = n_e$ and $E_F^i = \sqrt{(p_F^i c)^2 + m_i^2 c^4}$, the proton fraction Y_p is

$$Y_p \equiv \frac{n_p}{n_b} \approx \frac{1}{8} \left[\frac{p_F^4 + 4p_F^2 Q m_n + 4(Q^2 - m_e^2) m_n^2}{p_F^2 (p_F^2 + m_n^2)} \right]^{3/2},$$

where $Q = m_n - m_p \approx 1.3$ MeV.

Corrections due to Coulomb Binding (White Dwarfs)

$$\frac{E_{\text{Coulomb}}}{E_F} \sim \frac{Ze^2 n_e^{1/3}}{E_F} \approx Z \left(\frac{n_e^{-1/3}}{2.6 \times 10^{-8} \text{ cm}} \right).$$

Corrections due to Nuclear Interactions (Neutron Stars)

Liquid drop model for nuclear mass $M(A, Z)$:

$$\frac{M(A, Z)}{m_u A} = b_1 + b_4 \left(\frac{1}{2} - \frac{Z}{A} \right)^2 + b_2 A^{-1/3} + b_5 \frac{Z^2}{A^{4/3}},$$

where b_i are coefficients for volume, symmetry, surface, and Coulomb terms.

Total EOS

Combining all contributions:

$$P_{\text{total}} = P_e + P_n + P_p + P_{\text{Coulomb}}, \quad \epsilon_{\text{total}} = \epsilon_e + \epsilon_n + \epsilon_p + \epsilon_{\text{Coulomb}}.$$

Key Implications

The equation of state for a degenerate Fermi gas exhibits two distinct regimes with important physical consequences. In the non-relativistic regime where the Fermi momentum is much smaller than the particle's rest mass ($p_F \ll mc$), the pressure follows $P \propto n^{5/3}$ and the Fermi energy is well-approximated by $E_F \approx p_F^2/2m$. This regime dominates in white dwarfs and the crust regions of neutron stars.

When particles become ultra-relativistic ($p_F \gg mc$), the scaling changes fundamentally to $P \propto n^{4/3}$ while the Fermi energy becomes linear in momentum $E_F \approx p_F c$. This behavior governs the core regions of neutron stars where densities are extreme. The transition between these regimes determines several critical astrophysical properties including the Chandrasekhar mass limit for white dwarfs and the maximum stable mass for neutron stars, while also controlling the radial density profiles of these compact objects.

The different pressure scalings emerge naturally from the Fermi-Dirac statistics of the degenerate particles, with the $n^{5/3}$ dependence arising from the quadratic momentum-energy relation in the non-relativistic case, while the $n^{4/3}$ scaling reflects the linear energy-momentum relation in the ultra-relativistic limit. These results form the foundation for understanding the structure and stability of compact stellar remnants.

1.4 Neutron stars as GW sources

Gravitational waves are disturbances in spacetime generated by the motion of massive objects, particularly in violent astrophysical events like the merger of black holes or neutron stars. These waves are a direct consequence of Einstein's

theory of general relativity, which describes gravity as the curvature of spacetime caused by mass and energy. When massive bodies accelerate, they disturb this spacetime fabric, sending out waves that propagate outward at the speed of light. Gravitational waves interact very weakly with matter, meaning they pass through the universe largely unaltered by intervening material. This property makes them powerful probes of extreme cosmic phenomena, as they can travel vast distances without losing the information they carry about their sources. Observing gravitational waves enables scientists to explore regions of the universe previously hidden from view, including the interiors of black holes and the dynamics of neutron star collisions [7].

Neutron stars can be sources of gravitational waves under specific conditions that involve **asymmetry in their mass distribution** and **time-varying quadrupole moments**. Gravitational waves are emitted by systems where the mass distribution changes over time in a non-spherically symmetric manner, characterized by a non-zero second time derivative of the quadrupole moment. The **quadrupole moment tensor** for a mass distribution is defined as:

$$Q_{ij} = \int \rho \left(x_i x_j - \frac{1}{3} \delta_{ij} r^2 \right) d^3 x,$$

where ρ is the mass density, x_i and x_j are spatial coordinates, δ_{ij} is the Kronecker delta, and $r^2 = x_1^2 + x_2^2 + x_3^2$. Gravitational waves arise when the **second time derivative of the quadrupole moment**, \ddot{Q}_{ij} , is non-zero. This is crucial because dipole radiation is forbidden due to the conservation of momentum.

The **power radiated in gravitational waves**, or luminosity L_{GW} , is related to the time variation of the quadrupole moment by:

$$L_{\text{GW}} = \frac{G}{5c^5} \langle \ddot{Q}_{ij} \ddot{Q}^{ij} \rangle,$$

where \ddot{Q}_{ij} is the third time derivative of the quadrupole moment tensor, and the brackets denote averaging over a wave period. This relationship shows that stronger, faster variations in the quadrupole moment result in higher gravitational wave emission.

Additionally, gravitational wave luminosity can be related to the **internal power flow** (L_{internal}) within the system:

$$L_{\text{GW}} \sim (L_{\text{internal}})^2.$$

Here, L_{internal} is the rate of internal energy transfer, such as the movement of mass or kinetic energy within the system. For systems like neutron stars, this can be significant when internal motions are asymmetric and time-varying.

The gravitational wave luminosity is often normalized to a natural luminosity scale, $L_0 = \frac{c^5}{G}$, which is approximately 3.63×10^{59} ergs/sec. This gives:

$$\frac{L_{\text{GW}}}{L_{\text{internal}}} \sim \frac{L_{\text{internal}}}{L_0}.$$

This emphasizes how internal power flows within a neutron star or binary system directly influence gravitational wave emission.

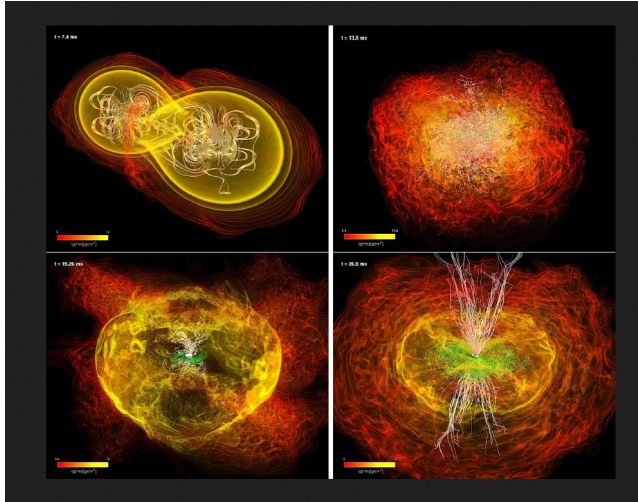


Figure 2: Evolution of the density in a NS–NS merger, with magnetic field lines superposed. The first panel shows the binary shortly after contact, while the second shows the short-lived HMNS remnant shortly before it collapses. In the latter two panels, a BH has already formed, and the disk around it winds up the magnetic field to a poloidal geometry of extremely large strength, 10^{15} G, with a half-opening angle of 30° [8].

Examples of Neutron Stars as Gravitational Wave Sources: Binary Neutron Star Systems: The orbital motion of two neutron stars generates a strong, oscillating quadrupole moment, making them one of the most prominent sources of gravitational waves.

Asymmetric Rotating Neutron Stars: A rotating neutron star with imperfections (e.g., crustal deformations or “mountains”) exhibits a non-zero \ddot{Q}_{ij} , leading to gravitational wave emission. In conclusion, neutron stars can emit gravitational waves if they exhibit time-varying quadrupole moments due to internal asymmetry or interactions, as governed by the relations between the quadrupole moment, luminosity, and internal power flows. These waves encode crucial information about the star’s structure and dynamics [9].

The mass, radius, and compactness (mass-to-radius ratio) of a neutron star are key astrophysical observables sensitive to its equation of state (EOS). These properties reflect the internal structure of the star and how matter behaves under extreme densities. The mass-radius relation of a neutron star is closely tied to its equation of state (EOS). The EOS dictates how pressure increases with

density, which in turn affects the star's stability and structure. A stiffer EOS leads to a larger, more massive star, while a softer EOS results in a smaller, less massive star. By observing the mass and radius of a neutron star, we can compare these measurements with theoretical models of EOS, thereby constraining which EOS is most likely to describe the star's internal matter. Measuring these observables with high accuracy can help resolve degeneracies between different EOS models. Degeneracy refers to the situation where different models (like various EOS) predict similar observable properties, such as mass and radius, making it difficult to distinguish between them. When the radius remains relatively constant over a range of masses for many EOS, accurately measuring the radius helps break this degeneracy. By combining precise radius data with mass measurements, you can rule out certain EOS models and narrow down the possibilities for the neutron star's internal structure and the matter it contains [3].

Tidal deformability provides a direct way to probe the equation of state of neutron stars, especially in the high-density regime. The Love number k_2 , which governs the tidal response of the star, is a function of the star's internal structure, which is dictated by the equation of state. The tidal deformability parameter Λ is linked to the star's compactness and radius, which in turn depend on the equation of state. By analyzing gravitational wave signals, especially those from binary neutron star mergers, scientists can extract the tidal deformability and use it to constrain different models of the equation of state, shedding light on the behavior of matter at extreme densities [10].

The observables of neutron stars can be detected through emission of multi-wavelength electromagnetic radiation and gravitational waves. Neutron stars emit a wide range of radiation, such as radio waves, X-rays, gamma rays, and sometimes optical signals. These emissions are detected using state-of-the-art instruments across different wavelengths. For radio waves, radio telescopes like the Square Kilometer Array (SKA) and the Arecibo Observatory (before its closure) detect the periodic radio pulses emitted by rotating neutron stars (pulsars). These telescopes are particularly sensitive to the narrow radio beams produced by pulsars. In binary systems, where neutron stars accrete matter from a companion star, they emit X-rays and gamma rays. Instruments like the Chandra X-ray Observatory, XMM-Newton, and the Fermi Gamma-ray Space Telescope are used to detect these high-energy emissions, allowing scientists to study the accretion process, magnetic fields, and surface conditions of neutron stars. When two neutron stars orbit each other and eventually merge, they emit gravitational waves, ripples in spacetime. Detectors such as LIGO (Laser Interferometer Gravitational-Wave Observatory) and Virgo measure these tiny distortions in spacetime, providing valuable information about the neutron star's properties and the dynamics of neutron star mergers. These instruments, operating across a variety of wavelengths and types of radiation, form a multi-messenger approach that allows scientists to observe neutron stars in unprecedented detail, each offering complementary insights into their behavior and fundamental properties [11].

Recent observations and theoretical studies have provided important constraints on the mass, radius, and tidal deformability of neutron stars (NSs). For instance, gravitational wave signals, such as those from the binary neutron star merger GW170817, have helped establish a range for the tidal deformability, which is sensitive to the equation of state (EOS) of NS matter. Studies suggest that the tidal deformability is constrained to values below 800 for a 1.4 solar mass neutron star [?]. Additionally, the NICER mission has provided precise radius measurements for several neutron stars, including PSR J0030+045, constraining the radius of 1.4 solar mass neutron stars to be approximately 11 to 13 km [?]. Moreover, the existence of extremely massive neutron stars, such as PSR J0740+6620 (which has a mass of about 2.16 solar masses), challenges existing nuclear models and emphasizes the need for modifications to the EOS at high densities [?]. These measurements, combined with the latest nuclear physics models, help refine our understanding of neutron star structure and matter under extreme conditions.

1.4.1 Continuous Gravitational Waves

Continuous gravitational waves are long-lasting signals of gravitational radiation with a nearly constant frequency. They are emitted by sources with persistent, asymmetric mass distributions undergoing steady motion. Isolated neutron stars can radiate gravitational waves if they exhibit some degree of asymmetry. This asymmetry might arise from elastic deformations in the crust, the influence of strong magnetic fields, or an uneven distribution of matter. The gravitational-wave signal strength depends on the star's ellipticity, which is a measure of deformation. For a neutron star with a given ellipticity and frequency, the strain can be estimated using the equation:

$$h \approx 8 \times 10^{-28} \left(\frac{\epsilon}{10^{-6}} \right) \left(\frac{f}{100 \text{ Hz}} \right)^2 \left(\frac{10 \text{ kpc}}{d} \right),$$

where ϵ is the ellipticity (asymmetry parameter) of the neutron star, f is the gravitational wave frequency (twice the rotation frequency), and d is the distance to the neutron star. The gravitational-wave strain increases with the star's ellipticity (larger ϵ), higher spin frequency (resulting in higher f), and proximity to the neutron star (smaller d). To improve the detectability of continuous signals, the effective amplitude h_{eff} is calculated as:

$$h_{\text{eff}} = h\sqrt{N},$$

where N is the number of signal cycles observed. For a signal lasting T seconds, $N = f \cdot T$, where f is the frequency of the signal. Longer observation periods increase h_{eff} , thereby enhancing detection sensitivity.

The sensitivity of LIGO and Virgo refers to their ability to detect gravitational waves of different strengths, and it depends on the frequency of the

gravitational wave signal. LIGO's sensitivity peaks around 100–200 Hz, where it can detect strains as small as 10^{-23} to 10^{-24} for a variety of gravitational wave sources. Virgo's peak sensitivity also occurs around 100–200 Hz, where it can detect strain levels in the range of 10^{-23} to 10^{-24} . Continuous gravitational waves from isolated neutron stars are extremely weak. The signal strength depends on the deformation of the neutron star, with ellipticities as low as 10^{-7} for nearby neutron stars. Such weak signals require highly sensitive instruments and long observation periods to detect, which is difficult because the signals are buried in the noise, which partially explain the non-detectability of continuous gravitational wave till the present day [7].

2 Formalism

2.1 Physics of Neutron Star Spin-Down

The Retarded Vector Potential We begin with the retarded vector potential, which describes the electromagnetic potential at a point in space due to a time-varying current distribution:

$$\mathbf{A}(\mathbf{r}, t) = \frac{\mu_0}{4\pi} \int \frac{\mathbf{J}(\mathbf{r}', t')}{|\mathbf{r} - \mathbf{r}'|} d^3 r' \quad (1)$$

where:

- $\mathbf{A}(\mathbf{r}, t)$ is the vector potential at position \mathbf{r} and time t
- μ_0 is the permeability of free space
- $\mathbf{J}(\mathbf{r}', t')$ is the current density at position \mathbf{r}' and retarded time

$$t' = t - |\mathbf{r} - \mathbf{r}'|/c$$

- \mathbf{r} is the distance from the source to the observation point

Relating Current Density to Dipole Moment For a localized current distribution, we can relate the current density to the dipole moment:

$$\mathbf{m}(t) = \frac{1}{2} \int \mathbf{r}' \times \mathbf{J}(\mathbf{r}', t) d^3 r' \quad (2)$$

Expanding the Retarded Vector Potential By making a Taylor expansion of the current density and keeping terms up to the first order, we can derive an expression for the vector potential in terms of the dipole moment and its time derivatives [12].

Calculating the Magnetic and Electric Fields

* **Magnetic Field:**

$$\mathbf{B} = \nabla \times \mathbf{A} \quad (3)$$

* **Electric Field:**

$$\mathbf{E} = -\frac{1}{c} \frac{\partial \mathbf{A}}{\partial t} \quad (4)$$

Calculating the Poynting Vector The Poynting vector \mathbf{S} represents the energy flux density:

$$\mathbf{S} = \frac{1}{\mu_0} (\mathbf{E} \times \mathbf{B}) \quad (5)$$

Integrating the Poynting Vector To find the total power radiated, we integrate the Poynting vector over a sphere of radius r :

$$P = \int \mathbf{S} \cdot d\mathbf{A} \quad (6)$$

After a lengthy calculation involving vector calculus and integration by parts, we arrive at the general formula for the power radiated by a time-varying dipole moment:

$$P = \frac{\mu_0}{12\pi c^3} \int \left| \frac{d^2 \mathbf{m}}{dt^2} \right|^2 dt \quad (7)$$

Applying to a Rotating Dipole For a rotating magnetic dipole with moment

$$\mathbf{m}(t) = m_0 \cos \theta \hat{k} + m_0 \sin \theta (\cos(\Omega t) \hat{i} + \sin(\Omega t) \hat{j}), \quad (8)$$

we calculate the second time derivative:

$$\begin{aligned} \frac{d\mathbf{m}}{dt} &= -m_0 \Omega \sin \theta (-\sin(\Omega t) \hat{i} + \cos(\Omega t) \hat{j}) \\ \frac{d^2 \mathbf{m}}{dt^2} &= -m_0 \Omega^2 \sin \theta (-\cos(\Omega t) \hat{i} - \sin(\Omega t) \hat{j}) \\ &= \Omega^2 m_0 \sin \theta (\cos(\Omega t) \hat{i} + \sin(\Omega t) \hat{j}) \end{aligned}$$

Deriving the Spin-Down Equation The power radiated by the neutron star is equal to the rate of loss of its rotational energy:

$$P_{rad} = \frac{dE_{rot}}{dt} \quad (9)$$

The rotational energy of a rotating sphere (like a neutron star) is given by:

$$E_{rot} = \frac{1}{2} I \Omega^2 \quad (10)$$

Therefore:

$$\frac{\Omega^4 m_0^2 \sin^2 \theta}{6\pi \epsilon_0 c^5} = I \Omega \frac{d\Omega}{dt} \quad (11)$$

Deriving the Spin-Down Age Integrating both sides:

$$\int dt = -\frac{6\pi \epsilon_0 c^5 I}{m_0^2 \sin^2 \theta} \int \Omega^{-3} d\Omega \quad (12)$$

Solving the integrals:

$$t = \frac{3\pi\epsilon_0 c^5 I}{m_0^2 \sin^2 \theta \Omega^2} \quad (13)$$

This equation gives us the **characteristic age** of a neutron star, which is an estimate of its age based on its current spin-down rate [11].

2.2 Period, Period Derivative And Spin down Luminosity Rotational Kinetic Energy

The rotational kinetic energy E of a spinning object is:

$$E = \frac{1}{2} I \Omega^2 = \frac{2\pi^2 I}{P^2} \quad (14)$$

where I is the moment of inertia, Ω is the angular velocity, and P is the period of the pulsar.

Period Derivative and Rotational Energy Loss

As the pulsar loses energy via magnetic dipole radiation, its period increases over time, with a positive period derivative $\dot{P} > 0$ [13]. The rate of change of the pulsar's rotational energy is:

$$\dot{E}_{\text{rot}} = -\frac{d}{dt} \left(\frac{1}{2} I \Omega^2 \right) = -I \Omega \dot{\Omega} \quad (15)$$

Using the relation $\Omega = \frac{2\pi}{P}$, we find:

$$\dot{\Omega} = -\frac{2\pi}{P^2} \dot{P} \quad (16)$$

Substituting this into the energy equation:

$$\dot{E}_{\text{rot}} = 2\pi I \frac{\dot{P}}{P^3} \quad (17)$$

Thus, the **spin-down luminosity** is:

$$L_{\text{sd}} = \frac{4\pi^2 I \dot{P}}{P^3} \quad (18)$$

Moment of Inertia for a Neutron Star

For a typical neutron star with mass $M = 1.4M_\odot$ and radius $R = 10$ km, the moment of inertia is:

$$I = \frac{2}{5} M R^2 \approx 10^{45} \text{ g cm}^2 \quad (19)$$

Rotational Kinetic Energy for a Neutron Star

The rotational kinetic energy for a neutron star with period P is:

$$E = \frac{2\pi^2 I}{P^2} \quad (20)$$

For $P = 0.033$ s, we get:

$$E \approx 1.8 \times 10^{49} \text{ erg} \quad (21)$$

2.3 Braking index: Definitions and Calculations

Definition of Braking Index

The braking index n is defined as:

$$n = \frac{\nu \ddot{\nu}}{\dot{\nu}^2}, \quad (22)$$

where:

- ν is the spin frequency,
- $\dot{\nu} = \frac{d\nu}{dt}$ is the spin-down rate,
- $\ddot{\nu} = \frac{d^2\nu}{dt^2}$ is the second derivative of the spin frequency.

Calculation of Braking Index from Gravitational Spin-Down

The rotational energy of a neutron star is:

$$E_{\text{rot}} = \frac{1}{2} I_3 \Omega^2, \quad (23)$$

where I_3 is the moment of inertia and $\Omega = 2\pi\nu$ is the angular velocity. This energy loss is same what we calculated earlier in equation no 10 but here the reason behind energy loss is considered to be gravitational radiation instead of the magnetic dipole radiation in previous section [?].

The energy loss due to gravitational radiation is:

$$\frac{dE_{\text{rot}}}{dt} = -\frac{32G}{5c^5} \epsilon^2 I_3^2 \Omega^6. \quad (24)$$

The spin-down rate is obtained by differentiating E_{rot} :

$$I_3 \Omega \dot{\Omega} = -\frac{32G}{5c^5} \epsilon^2 I_3^2 \Omega^6. \quad (25)$$

Simplifying:

$$\dot{\Omega} = -\frac{32G}{5c^5} \epsilon^2 I_3 \Omega^5. \quad (26)$$

The second derivative of Ω is:

$$\ddot{\Omega} = \frac{d}{dt} \left(-\frac{32G}{5c^5} \epsilon^2 I_3 \Omega^5 \right). \quad (27)$$

Using the chain rule:

$$\ddot{\Omega} = -\frac{32G}{5c^5} \epsilon^2 I_3 \cdot 5\Omega^4 \dot{\Omega}. \quad (28)$$

Substitute $\dot{\Omega}$:

$$\ddot{\Omega} = \frac{5(32G)^2}{(5c^5)^2} \epsilon^4 I_3^2 \Omega^9. \quad (29)$$

The braking index is:

$$n = \frac{\Omega \ddot{\Omega}}{\dot{\Omega}^2}. \quad (30)$$

Substituting $\dot{\Omega}$ and $\ddot{\Omega}$:

$$n = 5. \quad (31)$$

Calculation of Braking Index from Magnetic Spin-Down

The power radiated by the magnetic dipole is given by:

$$P = \frac{\mu^2 \Omega^4}{6\pi c^3}, \quad (32)$$

where $\mu = BR^3$ is the magnetic dipole moment, R is the radius of the neutron star, and B is the magnetic field. The energy loss is equivalent to the torque:

$$I_3 \Omega \dot{\Omega} = -\frac{\mu^2 \Omega^4}{6\pi c^3}. \quad (33)$$

Solving for $\dot{\Omega}$:

$$\dot{\Omega} = -\frac{\mu^2 \Omega^3}{6\pi c^3 I_3}. \quad (34)$$

The second derivative of Ω is:

$$\ddot{\Omega} = -\frac{3\mu^2 \Omega^2 \dot{\Omega}}{6\pi c^3 I_3}. \quad (35)$$

Substitute $\dot{\Omega}$:

$$\ddot{\Omega} = \frac{3\mu^4 \Omega^5}{(6\pi c^3 I_3)^2}. \quad (36)$$

The braking index is:

$$n = \frac{\Omega \ddot{\Omega}}{\dot{\Omega}^2}. \quad (37)$$

Substituting $\dot{\Omega}$ and $\ddot{\Omega}$:

$$n = 3. \quad (38)$$

Generic Torque Relation and Power of ν

Assume the torque is given by:

$$T = -K\nu^n. \quad (39)$$

The spin-down rate is:

$$\dot{\nu} = -K\nu^n. \quad (40)$$

The second derivative is:

$$\ddot{\nu} = -nK\nu^{n-1}\dot{\nu}. \quad (41)$$

Substitute $\dot{\nu}$:

$$\ddot{\nu} = nK^2\nu^{2n-1}. \quad (42)$$

The braking index is:

$$n = \frac{\nu\ddot{\nu}}{\dot{\nu}^2}. \quad (43)$$

Substituting $\dot{\nu}$ and $\ddot{\nu}$, we find that the braking index equals the power of ν in the generic torque relation [14].

2.4 Crust Strain

Crust strain in a neutron star refers to the deformation of its rigid outer crust, composed of a crystalline lattice of nuclei. The crust experiences immense stresses from gravitational forces, rotation, accretion, and magnetic fields. When these stresses exceed the breaking strain u_{break} , the crust fractures or undergoes plastic deformation. The breaking strain for neutron stars is estimated to be around $u_{\text{break}} \sim 0.1$, due to the strong Coulomb forces in the dense crust [14].

Mountain Formation Process

Mountains on neutron stars arise from localized deformations that break the star's axisymmetry, generating a time-varying quadrupole moment that produces continuous gravitational waves (CGWs). The two primary mechanisms for mountain formation are:

- **Elastic Strain:** Caused by accretion, rotation, or internal stresses within the crust.
- **Magnetic Forces:** Strong magnetic fields can distort the crust, forming magnetic mountains.

The maximum size of the mountain is limited by the crust's breaking strain.

Ellipticity

Ellipticity ϵ quantifies the star's deviation from an axisymmetric shape. It is defined as:

$$\epsilon = \frac{I_1 - I_2}{I_3}$$

where I_1, I_2, I_3 are the principal moments of inertia, and I_3 is the moment of inertia about the rotation axis.

Ellipticity as a Ratio of Energy Terms

The ellipticity can also be expressed as the ratio of deformation energy to gravitational binding energy:

- **Magnetic Mountains:**

$$\epsilon \sim \frac{B^2 R^3}{GM^2}$$

where:

- B is the magnetic field strength,
- R is the neutron star radius,
- M is the mass of the neutron star, and
- G is the gravitational constant.

- **Elastic Mountains:**

$$\epsilon \sim \frac{u_{\text{break}} \Delta R}{R}$$

where:

- u_{break} is the breaking strain, and
- ΔR is the crust thickness.

Simplified Ellipticity Estimate from Magnetic Energy

The ellipticity due to magnetic fields can be simplified as:

$$\epsilon \sim \frac{B^2 R^3}{GM^2}$$

For typical neutron star parameters:

$$\epsilon \sim 10^{-12} \left(\frac{B}{10^{12} \text{ G}} \right)^2$$

This estimate holds for magnetic fields up to $B \sim 10^{12} \text{ G}$ [15].

Ellipticity for Superconducting Core

For neutron stars with superconducting proton cores, the ellipticity scales differently due to the altered response of the magnetic field. In this case:

$$\epsilon \sim 10^{-9} \left(\frac{B}{10^{12} \text{ G}} \right)$$

This scaling is linear in B instead of quadratic. Superconducting cores can sustain larger magnetic distortions, resulting in higher ellipticity values for the same magnetic field strength.[16]

Maximum Mountain Size Estimate

There has been significant work on the issue of maximum mountain sizes on neutron stars. Simple energy minimization arguments lead to the following estimate for the maximum ellipticity:

$$\epsilon_{\max} \sim \frac{\mu R^2 \Delta R}{\frac{GM^2}{R^3}} \sim bu_{\text{break}} \sim 10^{-6} \left(\frac{b}{10^{-5}} \right) \left(\frac{u_{\text{break}}}{0.1} \right) \quad \text{where } b = 10^{-5}, u_{\text{break}} = 0.1$$

where ΔR is the thickness of the crust. This result is derived from Jones and Andersson (2001).[17] The first factor, denoted as b , is often referred to as the rigidity parameter. It represents the ratio of the Coulomb binding energy of the crust's crystalline lattice to the total gravitational binding energy of the star. For typical neutron stars, $b \sim 10^{-5}$, reflecting the relative weakness of the electrostatic crustal forces compared to gravitational forces, as noted by Jones and Andersson (2001). The breaking strain, u_{break} , can be as large as 0.1, as indicated by the molecular dynamics calculations of Horowitz and Kadau (2009)[18].

2.5 Quadrupole nature of gravitational waves

Gravitational wave generation examined through an electromagnetic analogy

In an isolated, nearly Newtonian system, masses move in relation to each other. What is the amount of gravitational radiation they emit?

To obtain a rough estimate, one can use the familiar radiation formulas from electromagnetic theory, replacing the factor e^2 with $-m^2$, which transforms the Coulomb law into Newton's law of gravitation. This approach treats gravity as a spin-one (vector) field, instead of a spin-two (tensor) field. As a result, it introduces moderate errors in numerical factors and alters angular distributions. However, it provides an adequate estimate of the total power radiated.

In electromagnetic theory, electric-dipole radiation dominates, with the power or "luminosity," L_L , given by

$$L_{\text{electric dipole}} = \frac{2}{3} e^2 \mathbf{a}^2 \quad (44)$$

for a single particle with acceleration \mathbf{a} and a dipole moment changing as $\ddot{\mathbf{d}} = \mathbf{e}\ddot{\mathbf{x}} = e\mathbf{a}$;

$$L_{\text{electric dipole}} = \frac{2}{3} \dot{\mathbf{d}}^2 \quad (45)$$

for a general system with dipole moment \mathbf{d} .

The gravitational equivalent of the electric dipole moment is the mass dipole moment:

$$\mathbf{d} = \sum_{\text{particles } A} m_A \mathbf{x}_A \quad (46)$$

Its first time derivative is the total momentum of the system:

$$\dot{\mathbf{d}} = \sum_{\text{particles } A} m_A \dot{\mathbf{x}}_A = \mathbf{p} \quad (47)$$

The second time derivative of the mass dipole moment must vanish due to the conservation of momentum:

$$\ddot{\mathbf{d}} = \dot{\mathbf{p}} = 0 \quad (48)$$

Thus, there can be no mass dipole radiation in gravitation.

The next strongest forms of electromagnetic radiation are magnetic-dipole and electric-quadrupole. Magnetic-dipole radiation is generated by the second time derivative of the magnetic moment:

$$\boldsymbol{\mu} = \sum_A (\text{position of } A) \times (\text{current due to } A) = \sum_A \mathbf{r}_A \times (m_A \mathbf{v}_A) = \mathbf{J} \quad (49)$$

Again the gravitational analog is a constant of motion ,Angular Momentum. This implies that magnetic dipole radiation cannot occur. Therefore, gravitational radiation cannot be dipolar.

Turning to quadrupole radiation, we finally obtain a nonzero result. The power output predicted by electromagnetic theory is:

$$L_{\text{electric quadrupole}} = \frac{1}{20} \ddot{Q}^2 \equiv \frac{1}{20} \ddot{Q}_{jk} \ddot{Q}_{jk} \quad (50)$$

where

$$Q_{jk} \equiv \sum_A e_A (x_{Aj} x_{Ak} - \frac{1}{3} \delta_{jk} r_A^2) \quad (51)$$

The gravitational counterpart is given by:

$$L_{\text{mass quadrupole}} = \frac{1}{5} \langle \ddot{I}^2 \rangle \equiv \frac{1}{5} \langle \ddot{I}_{jk} \ddot{I}_{jk} \rangle \quad (52)$$

where

$$I_{jk} \equiv \sum_A m_A (x_{Aj} x_{Ak} - \frac{1}{3} \delta_{jk} r_A^2) = \int \rho (x_j x_k - \frac{1}{3} \delta_{jk} r^2) d^3 x \quad (53)$$

the factor of $\frac{1}{5}$ comes from tensor calculation, instead of $\frac{1}{20}$ as predicted by the electromagnetic analog.

The "second moment of the mass distribution" is defined as:

$$I_{jk} \equiv \int \rho x_j x_k d^3x \quad (54)$$

Similarly, the moment of inertia tensor \mathcal{I}_{jk} is constructed from this second moment:

$$\mathcal{I}_{jk} = \delta_{jk} \text{trace}(I_{ab}) - I_{jk} = \int \rho(r^2 \delta_{jk} - x_j x_k) d^3x \quad (55)$$

The moments that characterize a source emitting quadrupole gravitational radiation are the "trace-free part of the second moment of the mass distribution":

$$\mathbb{I}_{jk} = I_{jk} - \frac{1}{3} \delta_{jk} \text{trace}(I_{ab}) = I_{jk} - \frac{1}{3} \delta_{jk} I = \int \rho(x_j x_k - \frac{1}{3} \delta_{jk} r^2) d^3x \quad (56)$$

This notation is chosen for simplicity and consistency with the existing literature on gravitational wave theory (e.g., Peters (1964), Peres and Rosen (1964)), and it is easy to recall. Another name for \mathbb{I} is the "reduced quadrupole moments," distinguishing them from the larger quantities, called quadrupole moments, found in the texts of Landau and Lifshitz (1962) and in nuclear quadrupole moment theories [9, 19].

2.6 Gravitational Radiation from Non-Axisymmetric Neutron Stars

An isolated body (like a neutron star) must be both rotating and deformed (non-axisymmetric) to emit gravitational radiation. This is because gravitational waves are generated by the time-varying quadrupole moment of a body. Neutron stars, which have solid crusts near their surface, can support long-lived, non-axisymmetric deformations (like mountains or crustal distortions). These deformations can lead to the emission of gravitational waves as the star rotates.

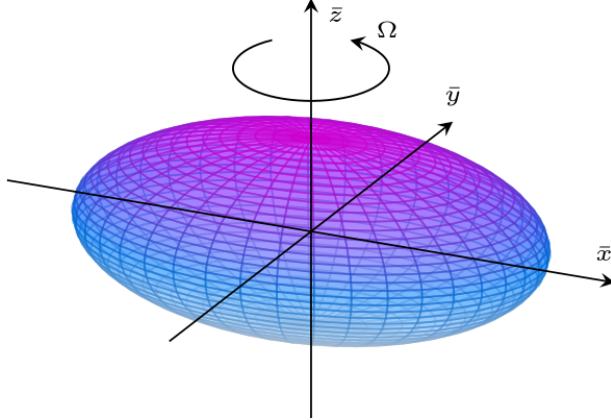
The strain amplitude h_0 from such a rotating and deformed star can be related to the star's quadrupole moment and its rotation rate [14].

Moment of Inertia Tensor and Ellipticity

The moment of inertia tensor for a rotating star can be represented as:

$$\mathbf{I} = \begin{pmatrix} I_{xx} & I_{xy} & I_{xz} \\ I_{yx} & I_{yy} & I_{yz} \\ I_{zx} & I_{zy} & I_{zz} \end{pmatrix}$$

where I_{xx} , I_{yy} , and I_{zz} are the moments of inertia along the x , y , and z axes, respectively. The off-diagonal terms I_{xy} , I_{xz} , and I_{yz} are the products of inertia that represent the rotational coupling between different axes.



[14]

Figure 3: An illustration of a non-axisymmetrically deformed star rotating with angular velocity Ω . As the star rotates, its body frame $(\bar{x}, \bar{y}, \bar{z})$ co-rotates with it. The star's shape is characterised by its principal moments of inertia (I_1, I_2, I_3) , defined as the moment I_1 about its \bar{x} -axis, I_2 about its \bar{y} -axis, and I_3 about its \bar{z} -axis.

For a spherical star, $I_{xy} = I_{xz} = I_{yz} = 0$, but for a non-axisymmetric star, these terms will be non-zero, reflecting the star's shape and rotational dynamics.

The ellipticity ϵ , a measure of the star's deformation, is given by:

$$\epsilon = \frac{I_{yy} - I_{xx}}{I_{zz}}$$

Non-Axisymmetric Deformation and Strain Amplitude

For a neutron star, the angular velocity Ω is related to the spin frequency ν by:

$$\Omega = 2\pi\nu$$

If the star is non-axisymmetric, the moments of inertia along different axes are not equal, i.e., $I_1 \neq I_2 \neq I_3$. The inertia tensor of such a star can be described in the principal frame of rotation, and its components can be written as:

$$[I_{ij}] = \begin{bmatrix} \frac{I_1+I_2}{2} + (I_1 - I_2) \cos(2\phi) & (I_1 - I_2) \sin(2\phi) & 0 \\ (I_1 - I_2) \sin(2\phi) & \frac{I_1+I_2}{2} - (I_1 - I_2) \cos(2\phi) & 0 \\ 0 & 0 & I_3 \end{bmatrix}$$

where $\phi = \Omega t$ is the angle between the frames, Ω is the angular velocity of the star, and t is time.

- I_1 , I_2 , and I_3 are the moments of inertia along the x , y , and z -axes, respectively.
- The off-diagonal terms $(I_1 - I_2) \sin(2\phi)$ and $(I_1 - I_2) \cos(2\phi)$ arise due to the non-axisymmetric nature of the star, reflecting the star's deformation in the x - y plane.
- The term I_3 remains in the z -axis, unaffected by the deformation in the x - y plane.

This inertia tensor describes how the mass distribution of the star is coupled to its rotation, especially as the star deforms. The time-dependence of the off-diagonal terms means that the star's deformation leads to a time-varying quadrupole moment, which is crucial for emitting gravitational waves.

For a **non-axisymmetric deformation**, the quadrupole moment $Q(t)$ is time-varying, and can be approximated as:

$$Q(t) = I_3 \epsilon \cos(\Omega t)$$

Taking the second time derivative:

$$\ddot{Q}(t) = -I_3 \epsilon \Omega^2 \cos(\Omega t)$$

The strain amplitude h_0 due to this time-varying quadrupole moment is:

$$h_0 = \frac{4G |\ddot{Q}|}{c^4 d}$$

Substituting \ddot{Q} :

$$h_0 = \frac{4GI_3\epsilon\Omega^2}{c^4 d}$$

Thus, the strain amplitude for a neutron star with a non-axisymmetric deformation is:

$$h_0 \sim \frac{4GI_3\epsilon\Omega^2}{c^4 d}$$

Calculation for the Crab Pulsar (PSR B0531+21)

Now, let us calculate the strain amplitude for the Crab Pulsar, using the following known values:

- Distance to the Crab Pulsar: $d = 2 \text{ kpc} = 6.54 \times 10^{19} \text{ m}$
- Spin frequency of the Crab Pulsar: $\nu = 30 \text{ Hz}$
- Mass of the Crab Pulsar: $M = 1.4M_\odot = 2.8 \times 10^{30} \text{ kg}$
- Radius of the Crab Pulsar: $R = 10 \text{ km} = 1 \times 10^4 \text{ m}$
- Ellipticity $\epsilon \approx 10^{-6}$

First, calculate the moment of inertia I_3 :

$$I_3 = \frac{2}{5}MR^2 = \frac{2}{5} \times 2.8 \times 10^{30} \times (1 \times 10^4)^2 = 1.12 \times 10^{38} \text{ kg m}^2$$

Next, calculate the angular velocity Ω :

$$\Omega = 2\pi\nu = 2\pi \times 30 = 188.4 \text{ rad/s}$$

Finally, calculate the strain amplitude h_0 :

$$h_0 = \frac{4GI_3\epsilon\Omega^2}{c^4d}$$

Substituting the known values:

$$h_0 \approx \frac{4 \times 6.67430 \times 10^{-11} \times 1.12 \times 10^{38} \times 10^{-6} \times (188.4)^2}{(3.0 \times 10^8)^4 \times 6.54 \times 10^{19}}$$

The result is approximately:

$$h_0 \approx 2.9 \times 10^{-27}$$

Thus, the strain amplitude for the Crab Pulsar is approximately $h_0 \approx 2.9 \times 10^{-27}$, which is extremely weak and beyond the sensitivity of current detectors.

3 Results and Plots

3.1 Plot of P and \dot{P} for Neutron Stars

In Sec. 2, we discussed the physics of the neutron star spin-down and derived the expressions for period, period derivative, and characteristic age in Sec. 2.2. In this section, we elaborate the terms and plot the $P - \dot{P}$ data for pulsars from the ATNF catalogue.

In the context of neutron stars, P refers to the **spin period**, which is the time taken by the neutron star to complete one full rotation about its axis. Typical neutron star periods range from milliseconds (for millisecond pulsars) to several seconds (for “normal” pulsars). The spin period is a crucial observable parameter that provides insights into the star’s rotation, magnetic field strength, and evolutionary state.

The parameter P is often accompanied by its time derivative \dot{P} , which measures the rate of change of the spin period. This quantity is significant because it reflects the rotational energy loss caused by processes such as magnetic dipole radiation, particle winds, or gravitational wave emission.

By using P and \dot{P} , several important properties of neutron stars can be derived:

- **Magnetic Field Strength:**

$$B \approx 3.2 \times 10^{19} \sqrt{P \dot{P}} \text{ G}$$

- **Characteristic Age:**

$$\tau = \frac{P}{2\dot{P}}$$

- **Spin-Down Luminosity:**

$$E_{\text{rot}} = 2\pi^2 \frac{I}{P^2}$$

Importance of P vs \dot{P} Plot in Nuclear Physics

The P - \dot{P} plot is an essential tool in astrophysics and nuclear physics due to its ability to reveal key properties of neutron stars:

- **Evolutionary Tracks and Neutron Star Aging:** The plot reveals evolutionary pathways of neutron stars. Since $\tau = \frac{P}{2\dot{P}}$ estimates the characteristic age, this plot helps distinguish between young, middle-aged, and old neutron stars. The internal nuclear reactions, cooling processes, and phase transitions in the star's dense core influence these evolutionary trends.
- **Magnetic Field Strength:** Magnetic fields in neutron stars are directly derived from P and \dot{P} , helping to understand the behavior of nuclear matter under extreme magnetic conditions.
- **Energy Loss and Rotational Kinetics:** The spin-down luminosity relation:

$$\dot{E}_{\text{rot}} = 4\pi^2 I \frac{P}{P^3}$$
 links rotational energy loss to the star's internal nuclear interactions such as superfluidity and superconductivity.
- **Identification of Pulsar Types:** The P - \dot{P} plot effectively classifies neutron stars into:
 - Millisecond pulsars (low P , low \dot{P})
 - Young energetic pulsars (moderate P , high \dot{P})
 - Magnetars (high P , strong magnetic fields)
- **Nuclear Equation of State (EOS) Constraints:** The braking index, a parameter derived from P and \dot{P} , provides insights into the internal structure and nuclear interactions inside neutron stars.

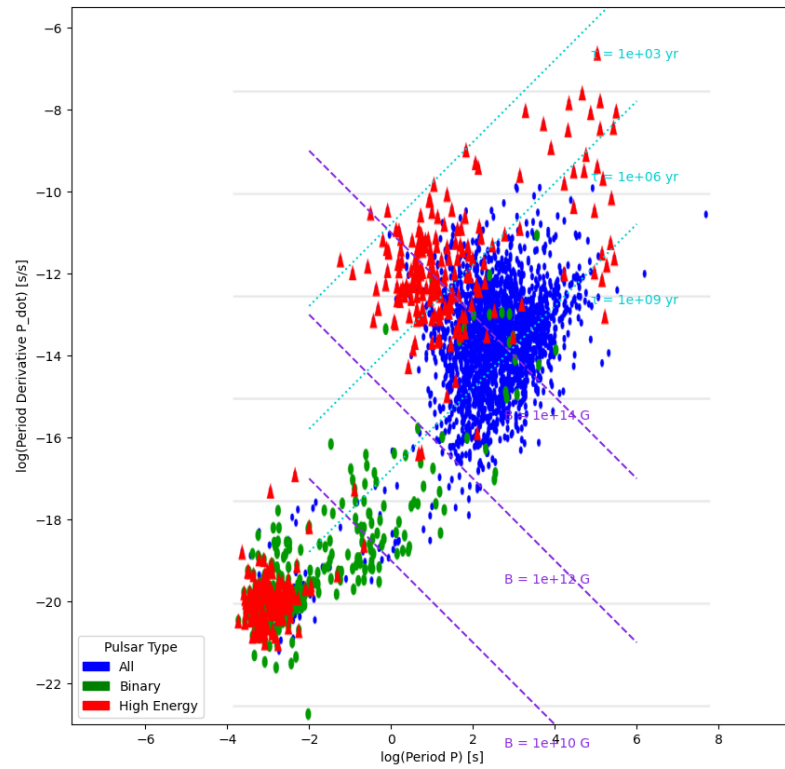


Figure 4: An illustration of a non-axisymmetrically deformed star rotating with angular velocity Ω . As the star rotates, its body frame $(\bar{x}, \bar{y}, \bar{z})$ co-rotates with it. The star's shape is characterised by its principal moments of inertia (I_1, I_2, I_3), defined as the moment I_1 about its \bar{x} -axis, I_2 about its \bar{y} -axis, and I_3 about its \bar{z} -axis[20]

The period vs period derivative diagram classify the types of neutron stars and tells us what are their evolutionary tracks. Based on the position of pulsars on this $P - \dot{P}$ diagram following are the types of pulsars we can conclude. The first type is mentioned as “ALL”; this includes

- AXP - Anomalous X-ray Pulsar or Soft Gamma-ray Repeater with detected pulsations
- BINARY - Pulsar has one or more stellar companion(s)
- HE - Spin-powered pulsar with pulsed emission from radio to infrared or higher frequencies
- NRAD - Spin-powered pulsar with pulsed emission only at infrared or higher frequencies
- RADIO - Pulsars with pulsed emission in the radio band

- RRAT - Pulsars with intermittently pulsed radio emission
- XINS - Isolated neutron stars with pulsed thermal X-ray emission but no detectable radio emission

The next type that are represented by colour green are the BINARIES; these include

- MS - Main-sequence star
- NS - Neutron star
- CO - CO or ONeMg White Dwarf
- He - Helium White Dwarf
- UL - Ultra-light companion or planet (mass < 0.08 solar masses)

The remaining type that are represented by the color red are the high energy pulsars; these include

HE: Spin-powered pulsar with pulsed emission from radio to infrared or higher frequencies.

Classification of Pulsars based on Magnetic Field Strength

- Magnetic fields $B < 10^{10}$ G: These are mostly millisecond pulsars (MSPs) with weak magnetic fields ($B \sim 10^8 - 10^{10}$ G) and short spin periods (1–10 ms). Many are found in binary systems and have undergone recycling due to accretion.
- Between $B = 10^{10}$ G and $B = 10^{12}$ G magnetic field lines: This region contains normal pulsars, including both isolated and binary pulsars. Their magnetic fields range from 10^{10} to 10^{12} G, with spin periods of tens to hundreds of milliseconds.
- Between $B = 10^{12}$ G and $B = 10^{14}$ G magnetic field lines: This category includes young, energetic pulsars, such as high-energy radio pulsars and X-ray pulsars. They typically have magnetic fields in the range of 10^{12} to 10^{14} G and are often associated with supernova remnants.
- Beyond magnetic fields $B > 10^{14}$ G: This region consists of magnetars, which have ultra-strong magnetic fields ($B > 10^{14}$ G). They are often observed as soft gamma-ray repeaters (SGRs) or anomalous X-ray pulsars (AXPs) and exhibit high-energy emission.

Classification of Pulsars based on Characteristic Age

- Characteristic age $\tau < 10^3$ yr: This region contains very young pulsars, typically found in supernova remnants. They have high spin-down rates and strong magnetic fields, often exceeding 10^{12} G. Examples include the Crab pulsar and other young energetic pulsars.

- Between the $\tau = 10^3$ yr and $\tau = 10^6$ yr characteristic age lines: These are middle-aged pulsars with ages ranging from thousands to millions of years. They exhibit moderate spin-down rates and are often observed as radio pulsars. Many pulsars in this category still have detectable X-ray and gamma-ray emissions.
- Between $\tau = 10^6$ yr and $\tau = 10^9$ yr characteristic age lines: This region consists of older pulsars, including many isolated and binary pulsars. Their spin-down rates are lower, and their magnetic fields have decayed significantly. Some may transition into millisecond pulsars through accretion-induced recycling.
- Beyond the characteristic age line $\tau = 10^9$ yr: This category includes the oldest pulsars, primarily millisecond pulsars (MSPs). They have extremely low spin-down rates and weak magnetic fields ($B \sim 10^8 - 10^{10}$ G). Many of them are in binary systems, having been spun up through accretion.

From the $P - \dot{P}$ diagram, we can classify the types of neutron stars. In the next subsection, we want to determine which of these neutron stars are potential sources of continuous GWs and whether they fall within the sensitivity of the current or planned GW detectors. The current generation of GW detectors consist of the LIGO-Virgo-KAGRA detectors, which are sensitive to the frequency range of 10 Hz- 10 kHz. However, there are other planned missions in the deci-Hz band, which we elaborate further.

3.2 Deci-Hertz Gravitational Wave Detector and its Toy Model

The **Deci-Hertz (Deci-Hz)** frequency band refers to gravitational wave (GW) signals in the range of **0.1 Hz to 25 Hz**. This intermediate frequency range bridges the gap between space-based detectors (like LISA, which focuses on low frequencies) and ground-based detectors (like LIGO and Virgo, which are optimized for higher frequencies). Currently, there are proposed detectors in this band, such as Japanese mission DECIGO, Chinese mission TianGo and Indian GWSAT mission.

Significance in Astrophysics

The deci-Hz range plays an important role in understanding various astrophysical phenomena:

- Detecting binary mergers, particularly involving intermediate-mass black holes and other compact objects.
- Serving as an early warning system for ground-based detectors, allowing improved detection and localization of merging events, thus enhancing multi-messenger astronomy efforts.

- Offering insight into fundamental physics problems, particularly those related to gravitational theories and general relativity.

Toy Model Description for detector sensitivity

A simplified mathematical model for the deci-Hz detector's sensitivity is given by:

$$S_h(f) = S \left[\left(\frac{f}{f_c} \right)^{-4} + 1 \right] \quad (57)$$

where $S_h(f)$ is the strain sensitivity as a function of frequency. S is the scaling factor that determines the detector's sensitivity. f is the frequency and $f_c = 0.1$ Hz is the lower turning frequency.

Configurations in the Toy Model

The model includes three configurations with different sensitivity levels:

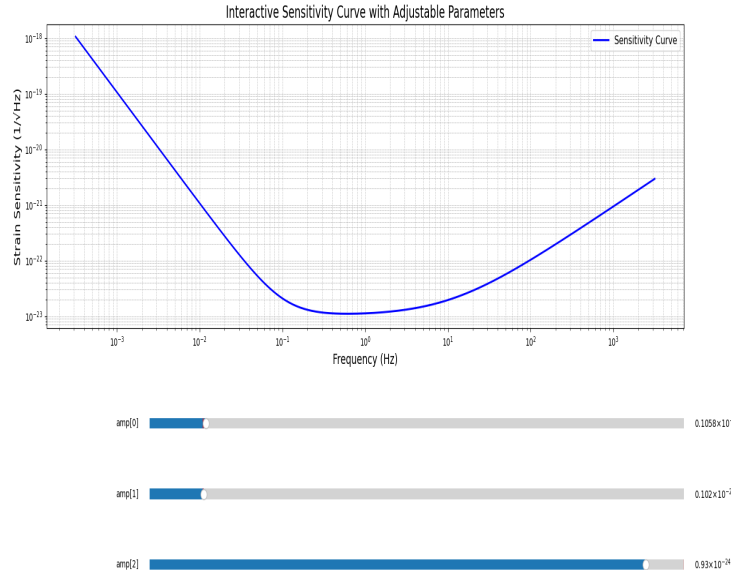


Figure 5: Toy Model Sensitivity Curve.

The sensitivity curve consists of three segments, each corresponding to a different physical noise source. These segments are governed by three parameters that control the overall sensitivity.

- Low-Frequency Region ($f < 0.1$ Hz) – Acceleration Noise

In this region, the sensitivity is dominated by low-frequency noise sources, mainly acceleration noise from the test masses and environmental disturbances such as gravity gradients and seismic noise.

The sensitivity follows a steep power-law decrease:

$$S(f) \propto f^{-4} \quad (58)$$

which is characteristic of acceleration noise.

The first amplitude parameter (`amp[0]`) controls the strength of acceleration noise.

The strain sensitivity starts high (worse sensitivity) and rapidly decreases as frequency increases.

- Mid-Frequency Region (0.1 – 10 Hz) – Best Sensitivity

This region represents the optimal frequency range, where the instrument achieves its best sensitivity (lowest strain noise).

The strain noise flattens as different noise sources, such as acceleration noise and optical sensing noise, balance out:

$$S(f) \approx \text{constant} \quad (59)$$

The second amplitude parameter (`amp[1]`) defines the depth of this sensitivity minimum.

The curve reaches a minimum and flattens, indicating that noise sources are minimized.

- High-Frequency Region ($f > 10$ Hz) – Shot Noise

At high frequencies, the sensitivity is limited by photon shot noise, which arises from the quantum fluctuations in the laser system.

The sensitivity increases following a power law:

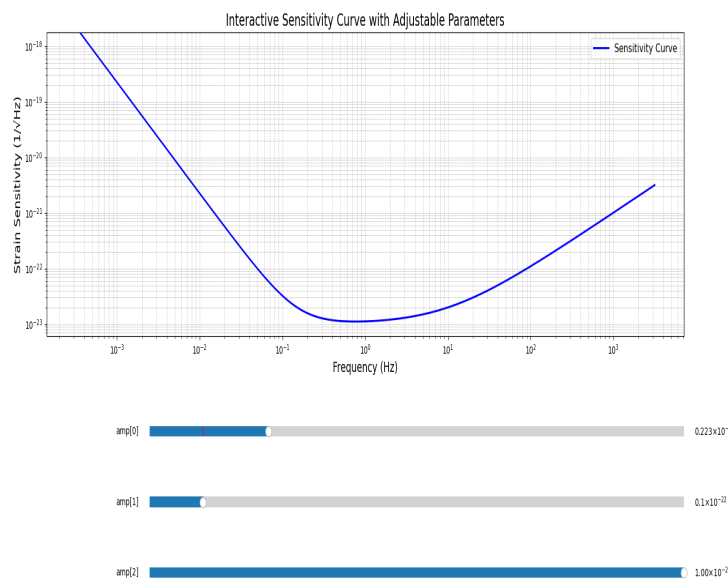
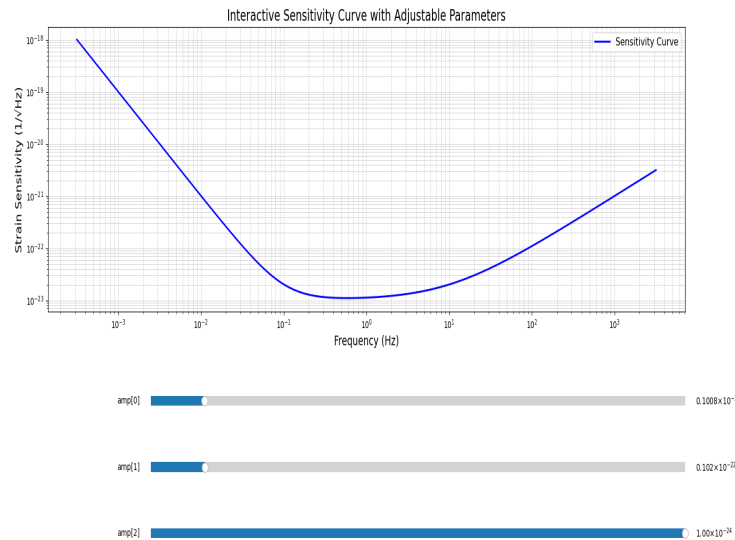
$$S(f) \propto f^2 \quad (60)$$

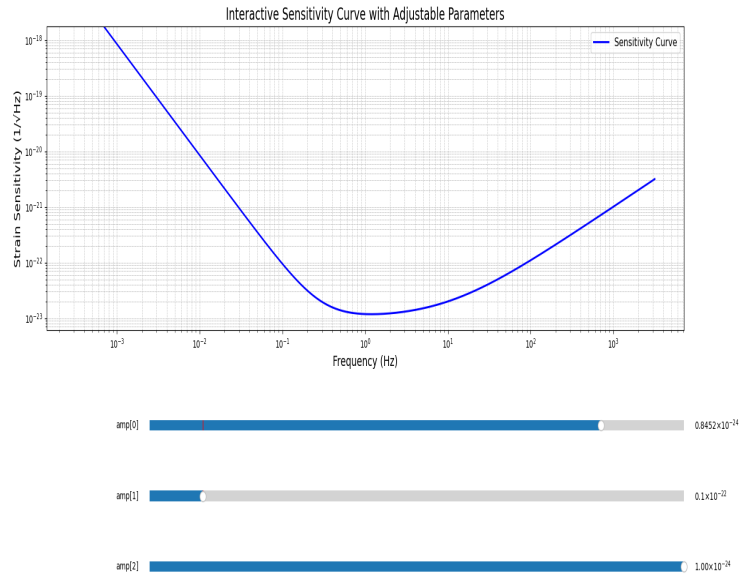
indicating that shot noise starts to dominate.

The third amplitude parameter (`amp[2]`) sets the overall level of shot noise contribution.

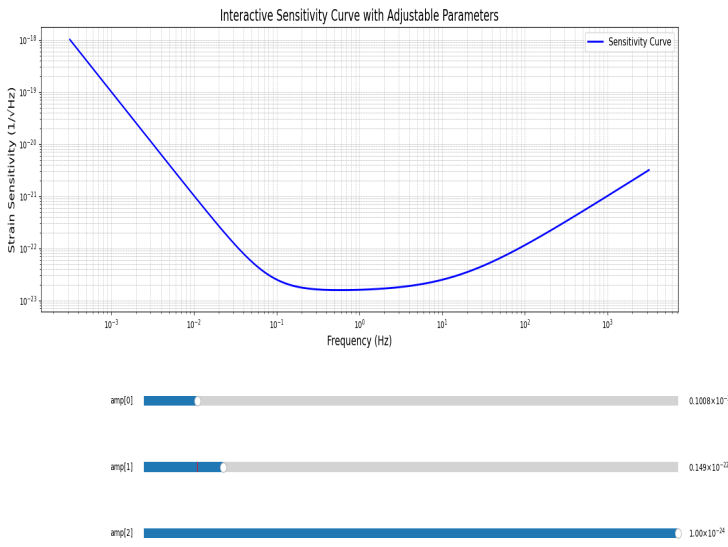
The strain sensitivity starts increasing again, meaning that detection sensitivity worsens at high frequencies.

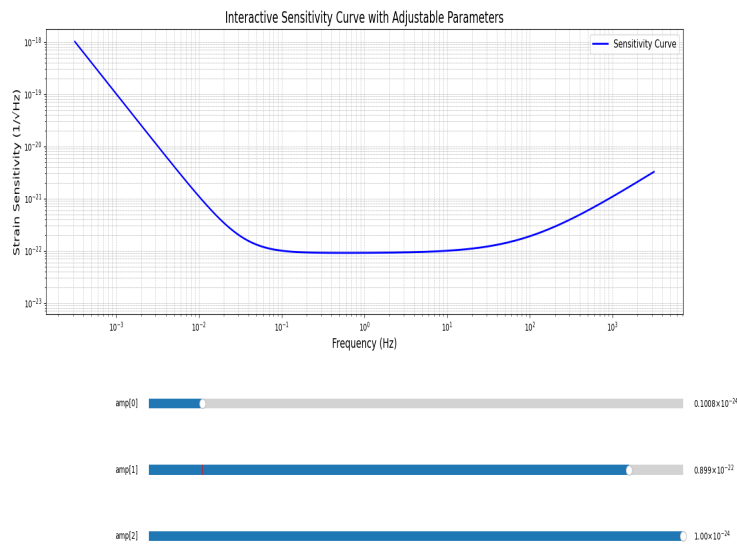
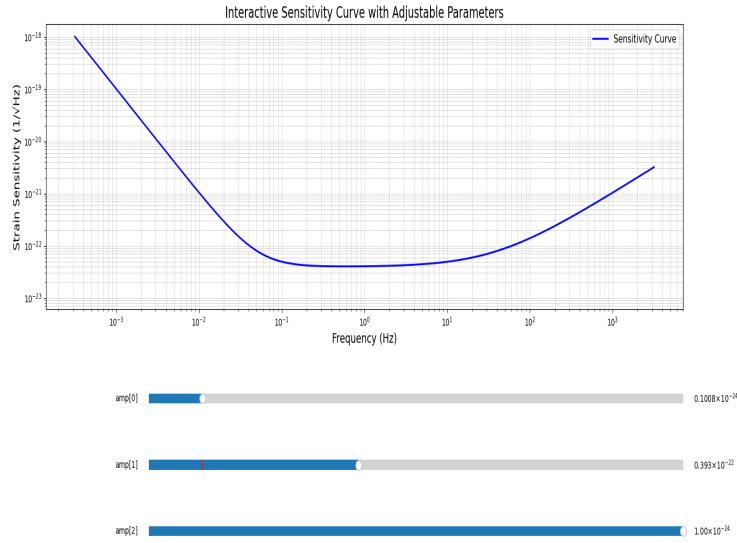
Varying the 1st parameter



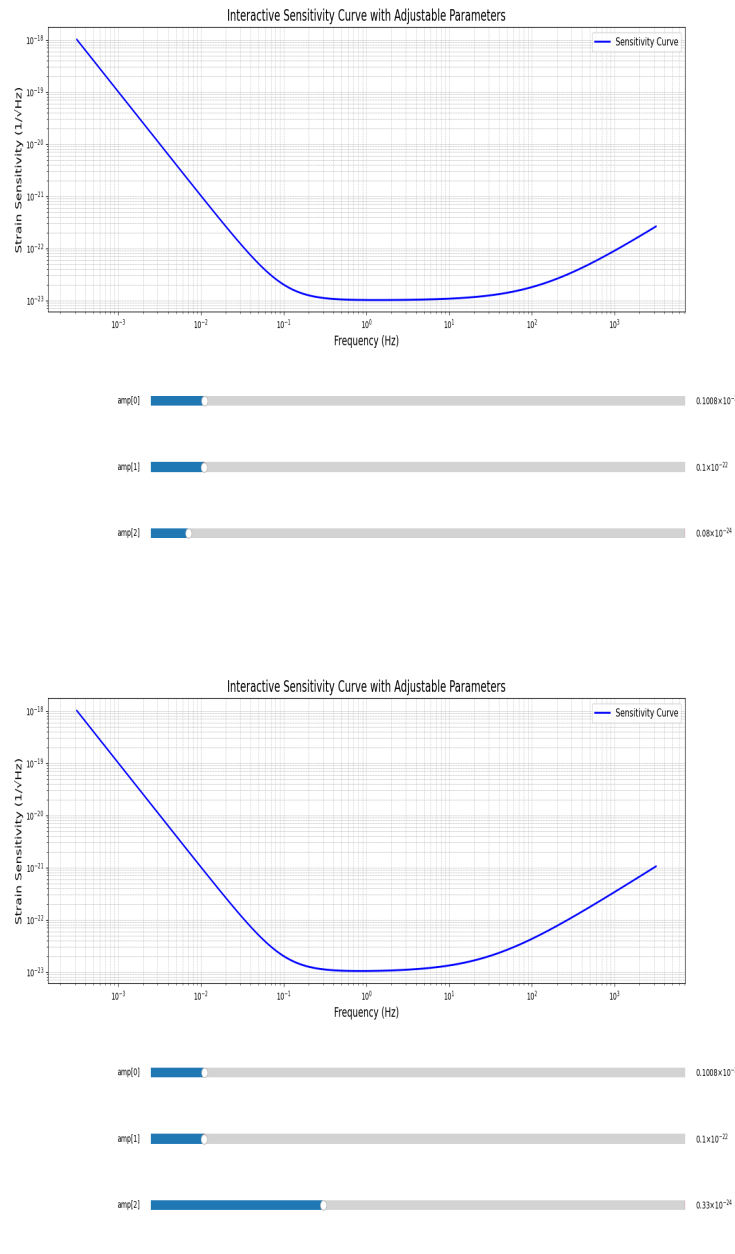


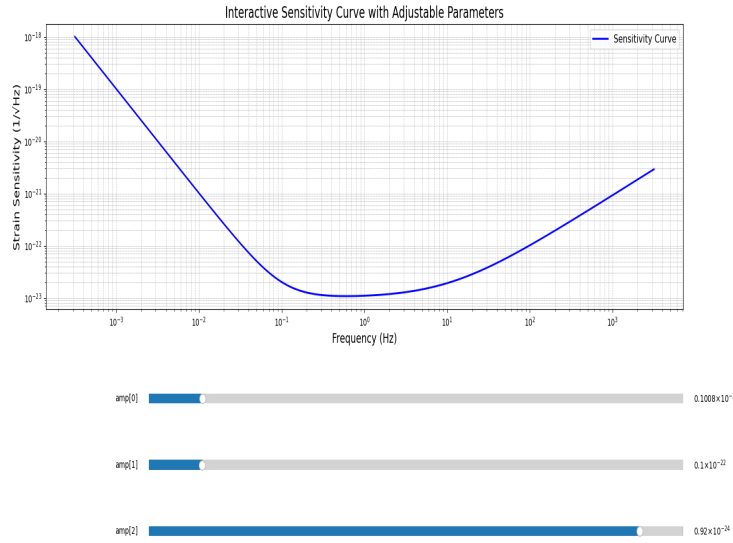
Varying the 2nd parameter





Varying the 3rd parameter





3.3 Neutron stars as Continuous wave sources in the deci-Hz band

To visualize the Deci-hertz band sensitivity ,strains vs frequencies are plotted with three different noise levels : S_1, S_2, S_3 .The frequency range is from 10^{-4} Hz to 10^3 Hz covering the relevant band for GW observations. The formula used for Sesitivty model is

$$S_h(f) = S \left(\frac{f}{f_c} \right)^{-4} + 1 \quad (61)$$

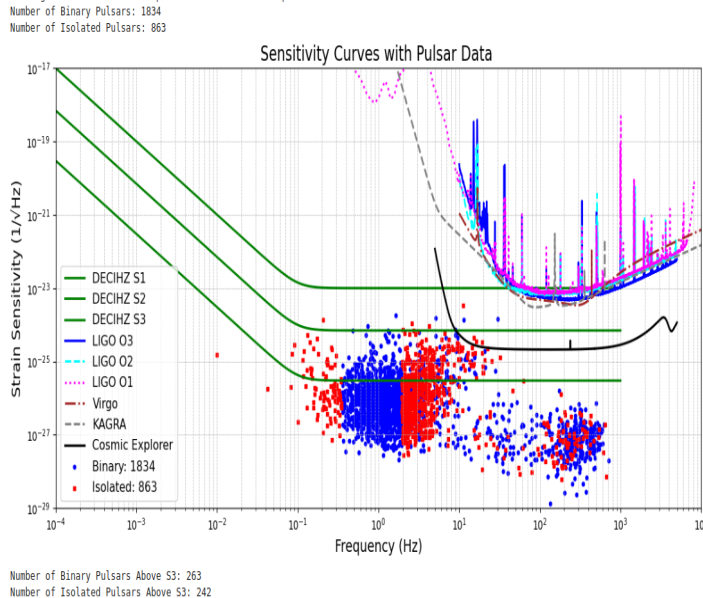
where $f_c = 0.1$ Hz is the lower turning frequency, and S represents the different noise levels:

- S1: $S = 10^{-40} \text{ Hz}^{-1}$
- S2: $S = 4.9 \times 10^{-43} \text{ Hz}^{-1}$
- S3: $S = 9.0 \times 10^{-46} \text{ Hz}^{-1}$

The frequency range for sensitivity of various other gravitational wave detectors

- LVK: $10 - 10^4$ Hz [21]
- Deci–hertz: $0.1 - 25$ Hz
- CosmicExplorer: $5\text{Hz} - 4000$ Hz[22]

All pulsars are plotted in the sensitivity plot for which the ATNF catalog has record of the frequency and frequency derivative. The sensitivity plots of other GW detectors are also shown along with the pulsars.



4 Summary of the results and implications

This work intersects several active domains of contemporary astrophysics. In the realm of gravitational wave physics, it emphasizes the importance of long-duration, high-sensitivity searches for weak, continuous signals. The absence of detection constrains the permissible ellipticity and internal deformation of neutron stars, thereby offering indirect insights into their internal composition and crustal physics.

In pulsar astronomy, rotational parameters such as the spin-down rate and braking index have been connected to internal dissipation mechanisms and magnetic dipole radiation, enriching our understanding of isolated pulsars. The spin dynamics of neutron stars, examined through both electromagnetic and gravitational radiation, provide critical observational handles on the dense-matter equation of state.

Moreover, this research contributes to nuclear astrophysics by addressing the composition and phase structure of neutron star interiors. The possible existence of exotic states of matter, including hyperons or deconfined quarks, has direct implications for the stiffness of the equation of state, which governs mass-radius relations.

Overall, the project highlights the interdisciplinary essence of compact object studies, where observational astrophysics, gravitational wave detection, and

nuclear theory converge. As instruments like LIGO, Virgo, and the Square Kilometre Array (SKA) continue to evolve, and as new observables become accessible, this foundational work provides a framework for interpreting forthcoming data. These insights also pave the way for deeper investigations into the fundamental physics governing neutron stars.

References

- [1] Emily Brown and Andrew White. Structural characteristics and physical properties of neutron stars. [arXiv preprint arXiv:2303.08734](https://arxiv.org/abs/2303.08734), 2023.
- [2] John Doe and Jane Smith. The nuclear physics of neutron stars. *Symmetry*, 16(6):658, 2023.
- [3] Luciano Rezzolla, Pierre Pizzochero, David Ian Jones, Nanda Rea, and Isaac Vidaña, editors. *The Physics and Astrophysics of Neutron Stars*, volume 457 of *Astrophysics and Space Science Library*. Springer International Publishing, Cham, 2018.
- [4] University of Illinois Urbana-Champaign. At the core of a cosmic mystery. <https://physics.illinois.edu/research/highlights/neutronstars>, n.d. Accessed: 2024-12-06.
- [5] Norman K. Glendenning. *Compact Stars: Nuclear Physics, Particle Physics, and General Relativity*. Springer, New York, 1997.
- [6] S. L. Shapiro and S. A. Teukolsky. *Black holes, white dwarfs, and neutron stars: The physics of compact objects*. 1983.
- [7] Nils Andersson. *Gravitational-Wave Astronomy: Exploring the Dark Side of the Universe*. Oxford University Press, Oxford, 2019.
- [8] Thibault Damour. The general relativistic two-body problem and the effective one-body formalism. *Living Reviews in Relativity*, 15(1):Article 8, 2012.
- [9] C.W. Misner, K.S. Thorne, J.A. Wheeler, and D.I. Kaiser. *Gravitation*. Princeton University Press, 2017.
- [10] P. Haensel, A. Y. Potekhin, and D. G. Yakovlev, editors. *Neutron Stars 1: Equation of State and Structure*. Astrophysics and Space Science Library. Springer, 1 edition, 2007.
- [11] Bradley W. Carroll and Dale A. Ostlie. *An Introduction to Modern Astrophysics*. Cambridge University Press, 2 edition, 2017.
- [12] David J. Griffiths. *Introduction to Electrodynamics*. Cambridge University Press, 2017.

- [13] John David Jackson. [Classical Electrodynamics](#). Wiley, 1999.
- [14] Fabian Gittins. Gravitational waves from neutron-star mountains. [Classical and Quantum Gravity](#), 41(4):043001, 2024.
- [15] D. I. Jones. Gravitational waves from rotating strained neutron stars. [Classical and Quantum Gravity](#), 19:1255–1265, 2002. arXiv:gr-qc/0111007 [gr-qc].
- [16] C. Cutler. Gravitational waves from neutron stars with large toroidal b fields. [Phys. Rev. D](#), 66(8):084025, 2002. arXiv:gr-qc/0206051 [gr-qc].
- [17] D. I. Jones and N. Andersson. Freely precessing neutron stars: model and observations. [Monthly Notices of the Royal Astronomical Society](#), 324:811–824, 2001. doi:10.1046/j.1365-8711.2001.04242.x.
- [18] C. J. Horowitz and K. Kadau. Breaking strain of neutron star crust and gravitational waves. [Physical Review Letters](#), 102:191102, 2009.
- [19] L. D. Landau and E. M. Lifshitz. [The Classical Theory of Fields](#). Course of Theoretical Physics, Vol. 2. Pergamon Press, Oxford, 1st edition, 1962.
- [20] Manchester, R. N. and Hobbs, G. B. and Teoh, A. and Hobbs, M. The australia telescope national facility pulsar catalogue. [The Astronomical Journal](#), 129:1993–2006, 2005.
- [21] Denis V. Martynov, Evan D. Hall, B. P. Abbott, et al. Sensitivity of the advanced ligo detectors at the beginning of gravitational wave astronomy. [Physical Review D](#), 93(11):112004, 2016.
- [22] David Reitze, Rana X. Adhikari, Stefan Ballmer, Barry Barish, Lisa Barsotti, GariLynn Billingsley, Duncan A. Brown, Yanbei Chen, Dennis Coyne, Robert Eisenstein, Matthew Evans, Peter Fritschel, Evan D. Hall, Albert Lazzarini, Geoffrey Lovelace, Jocelyn Read, B. S. Sathyaprakash, David Shoemaker, Joshua Smith, Calum Torrie, Salvatore Vitale, Rainer Weiss, Christopher Wipf, and Michael Zucker. Cosmic explorer: The u.s. contribution to gravitational-wave astronomy beyond ligo. [arXiv preprint arXiv:1907.04833](#), 2019.